Phonon-assisted upconversion photoluminescence of monolayer MoS$_2$ at elevated temperatures

FENGKAI MENG,[1] [ID] **XIAODONG YANG,[2] AND JIE GAO[1],***

[1]*Department of Mechanical Engineering, Stony Brook University, Stony Brook, NY 11794, USA*
[2]*Department of Mechanical and Aerospace Engineering, Missouri University of Science and Technology, Rolla, MO 65409, USA*
jie.gao.5@stonybrook.edu

Abstract: Upconversion photoluminescence (UPL) lies at the heart of optical refrigeration and energy harvesting. Monolayer transition metal dichalcogenides (TMDCs) have been identified as an excellent platform with robust phonon-exciton coupling for studying the phonon-assisted UPL process. Herein, we investigate the multiphonon-assisted UPL emission in monolayer MoS$_2$ at elevated temperatures and the temperature-dependent phonon contributions in the UPL process. When temperature goes up from 295 K to 460 K, the enhancement of the integrated UPL intensity is demonstrated due to the increased phonon population and the reduced phonon numbers involved in the UPL process. Our findings reveal the underlying mechanism of phonon-assisted UPL at high temperatures, and pave the way for the applications of photon upconversion in display, nanoscale thermometry, anti-Stokes energy harvesting, and optical refrigeration.

1. Introduction

In contrast to conventional downconversion photoluminescence (PL), upconversion photoluminescence (UPL) is an anti-Stokes process which emits a higher energy photon than that of the absorbed photon by gaining additional energy from the upconversion mechanism ranging from phonon absorption [1], multiphoton absorption [2] to Auger recombination [3]. Among all these mechanisms, phonon-assisted UPL is particularly attractive because it involves an efficient one-photon excitation process in the linear region, which can be achieved with continuous-wave (CW) laser excitation. The phenomena of phonon-assisted UPL have been extensively demonstrated in a variety of material systems, including quantum dots [4], nanoribbons [5], perovskite nanocrystals [6,7], color center in diamond [8], 2D materials and heterostructures [9,10]. Upconversion photon emission has been applied into a plenty of fields including optical tweezers [11], display [12], bioimaging [13], photothermal therapy [14], nanoscale thermometry [8], photodetectors [15], solar cells [16,17], photon avalanche [18], laser cooling [19,20], optical refrigeration [21], and energy harvesting [4]. 2D materials have attracted tremendous scientific interest in recent years since the discovery and development of mechanically exfoliated graphene [22–24]. In contrast to the zero-bandgap graphene, the emerging monolayer TMDCs of MoS$_2$, MoSe$_2$, WS$_2$ and WSe$_2$ possess direct bandgaps in visible and near-infrared (NIR) regions as well as strong binding energy of excitons, which have been extensively utilized in the integrated devices of photonics [25], nanoelectronics [26], and optoelectronics [27,28]. Monolayer TMDCs with strong photon-exciton and phonon-exciton interactions provide an intriguing platform for studying the phonon-assisted UPL process. Recently, considerable attention has been focused on the UPL processes in WSe$_2$ and WS$_2$ monolayers at low temperature and room temperature [1,29–31]. However, phonon-assisted UPL processes in TMDC monolayers above room temperature are not well explored yet. Additionally, monolayer MoS$_2$ with visible exciton emission offers the possibility of realizing NIR-to-visible photon upconversion.

Here, phonon-assisted photon upconversion from NIR to visible spectral range in monolayer MoS_2 at elevated temperatures is demonstrated. The linear power dependence of UPL intensity at both room temperature and high temperature is observed, which represents the one-photon anti-Stokes upconversion mediated by multiphonon absorption. UPL emission around 670 nm in the visible region with upconversion energy gain up to 221 meV is obtained at room temperature when monolayer MoS_2 is excited by a NIR 761 nm CW laser. As temperature goes up from 295 K to 460 K, a 62-fold enhancement of the integrated UPL intensity and a 27 nm redshift of the emission peak wavelength are achieved. The analysis of temperature-dependent UPL emission further explains the contributions of the increased phonon population and the reduced phonon number involved with UPL process at elevated temperatures. The monotonically increasing behavior of UPL emission intensity as a function of temperature is observed, which is distinct from the PL emission intensity exhibiting a combination of negative thermal quenching and normal thermal quenching processes. The demonstrated results of high-temperature phonon-assisted UPL process in monolayer MoS_2 have promising implications for applications in photon upconversion in display, nanoscale thermometry, anti-Stokes energy harvesting, and optical refrigeration.

2. Measurement and analysis of UPL process in monolayer MoS_2

Figure 1(a) shows the optical microscopic image of monolayer MoS_2 with the triangular size around 15 μm grown on sapphire substrate by chemical vapor deposition. The Raman spectrum measured by a 532 nm laser exhibits two strong Raman peaks at 388 cm^{-1} and 408 cm^{-1}, which indicates the in-plane vibrational phonon mode E_{2g}^1 and out-of-plane phonon mode A_{1g}, respectively. The peak separation of approximately 20 cm^{-1} between two Raman modes confirms the monolayer MoS_2 synthesis [32]. Figure 1(b) plots the PL spectrum of monolayer MoS_2 excited at 633 nm (black) and the UPL spectra excited at 725 nm (green) and 761 nm (red), respectively. It is shown that the peak wavelengths of UPL spectra are consistent with that of the PL emission, which are around 670 nm. Compared to the PL emission intensity, the UPL peak intensity excited at 725 nm and 761 nm is three and four orders of magnitude weaker, respectively. It is observed that the UPL peak intensity excited at 725 nm is about 15.8 times stronger than that excited at 761 nm. The weaker UPL emission intensity at 761 nm is attributed to the larger upconversion energy gain defined as $\Delta E = \hbar\omega_{UPL} - \hbar\omega_{exc}$, where $\hbar\omega_{UPL}$ is the UPL photon energy and $\hbar\omega_{exc}$ is the excitation photon energy. Upconversion energy gain is 140 meV under 725 nm excitation and reaches up to 221 meV with 761 nm excitation at room temperature. The upconversion energy gain is compensated by the multiphonon absorption process with $\Delta E = n\hbar\omega_{To}$, where n is the number of phonons and $\hbar\omega_{To}$ is the transverse optical (TO) phonon energy of A_{1g} mode (50 meV) in monolayer MoS_2. The achieved upconversion energy gain corresponds to 3-5 phonons involved in the phonon-assisted UPL process at room temperature.

The dependence of PL and UPL emission on the excitation power is characterized at both room temperature and elevated temperatures. Figure 2(a) and (b) depict the power-dependent PL spectra excited at 633 nm and UPL spectra excited at 761 nm of monolayer MoS_2 at room temperature, respectively. It shows that both Stokes and anti-Stokes emission spectra grow steadily with the increased excitation power. Figure 2(c) further plots the integrated emission intensity as a function of excitation power in a log-log scale at different excitation wavelengths. The solid lines show the data fitting with a power law $I = \alpha P^\beta$, where α is the fitting parameter, P is the excitation power and β is the exponent. The fitted exponent β is about 0.82, 0.92 and 0.97 for PL excited at 633 nm, UPL excited at 725 nm and 761 nm, respectively. All β values are close to 1, which infers that both the observed PL emission and UPL emission are attributed to one-photon linear processes. Furthermore, the measurement of UPL emission from monolayer MoS_2 as a function of excitation power is performed at elevated temperatures. As shown in Fig. 2(d) and (e), the UPL spectra under 761 nm excitation at 330 K and 380 K gradually increase with the
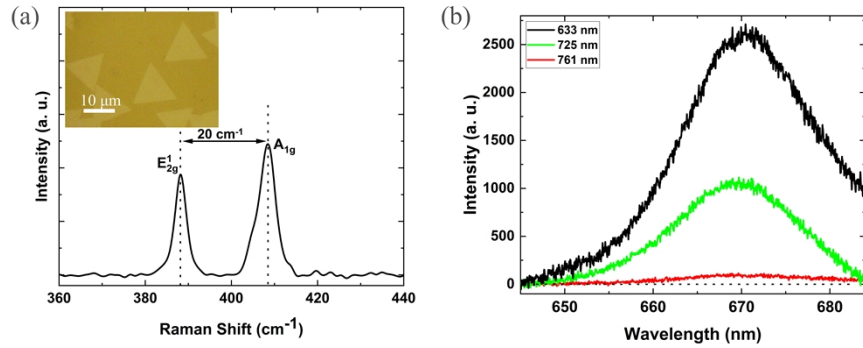
Fig. 1. (a) Raman spectrum of monolayer MoS_2 on sapphire showing the E^1_{2g} and A_{1g} phonon modes. The inset shows an optical microscopic image of the sample. (b) UPL and PL spectra from monolayer MoS_2 excited by 761 nm laser at 6.11 mW (red), 725 nm laser at 4.46 mW (green) and 633 nm laser at 5 µW (black).

excitation power. In Fig. 2(f), the power-dependent integrated UPL emission intensity is plotted at three elevated temperatures of 330 K, 380 K, and 430 K, exhibiting a linear power law behavior with fitted β values of 0.89, 0.95, and 1.15, respectively. This behavior is similar to the linear power dependence observed for UPL emission at room temperature. The power-dependent UPL characterizations indicate that the UPL emission in monolayer MoS_2 at both room temperature and elevated temperatures is a one-photon involved phonon-assisted process in the linear regime, ruling out the possibility of nonlinear optical process such as two-photon absorption [33] or auger recombination [34].
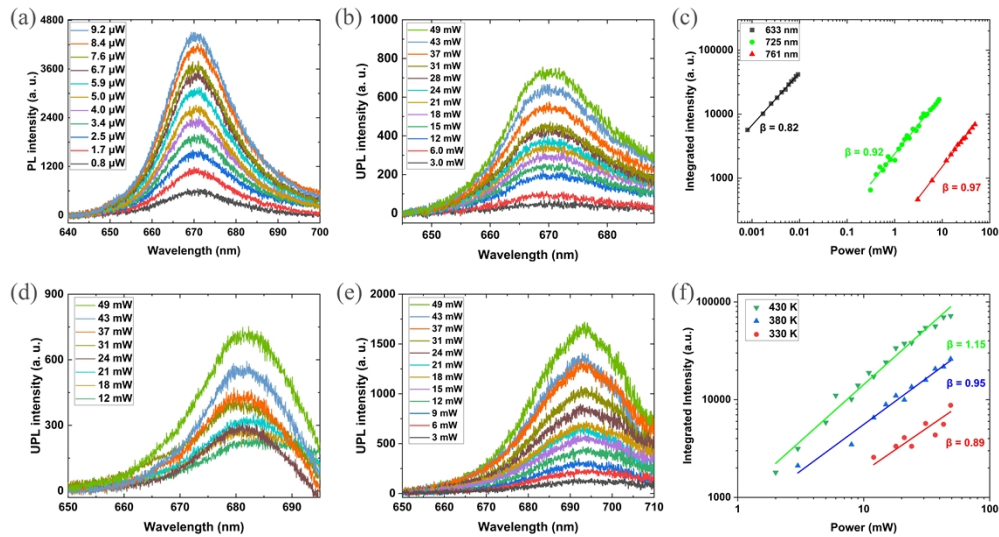
Fig. 2. Power dependence of (a) PL spectra excited at 633 nm and (b) UPL spectra excited at 761 nm of monolayer MoS_2 at room temperature. (c) Integrated PL intensity (black square) and UPL intensity excited at 725 nm (green dot) and 761 nm (red triangle) with respect to the excitation power. (d-e) Power-dependent UPL spectra measured at 330 K and 380 K. (f) Power dependence of integrated UPL intensity at 330 K (red dot), 380 K (blue up-pointing triangle) and 430 K (green down-pointing triangle), respectively.

In order to unveil the role of phonons in UPL process at elevated temperatures, temperature-dependent PL and UPL spectra of monolayer MoS$_2$ are measured as temperature increases from 295 K to 460 K. As illustrated in Fig. 3(a), the PL emission excited at 633 nm first gradually increases with the temperature until 320 K, and then continuously decreases with the temperature. The PL emission peak intensity at 460 K is reduced by 4.4 times than that at 320 K, dominated by thermal quenching effect. On the other hand, the UPL spectra excited at 761 nm in Fig. 3(b) display a monotonic growth as a function of temperature. The dashed lines show the Gaussian-Lorentzian convolution (Voigt) fitting of the UPL spectra. For instance, the UPL emission peak intensity at 460 K is 21 times stronger than that at 320 K. Moreover, both PL and UPL emission peak wavelengths exhibit a continuous redshift with the increased temperature.
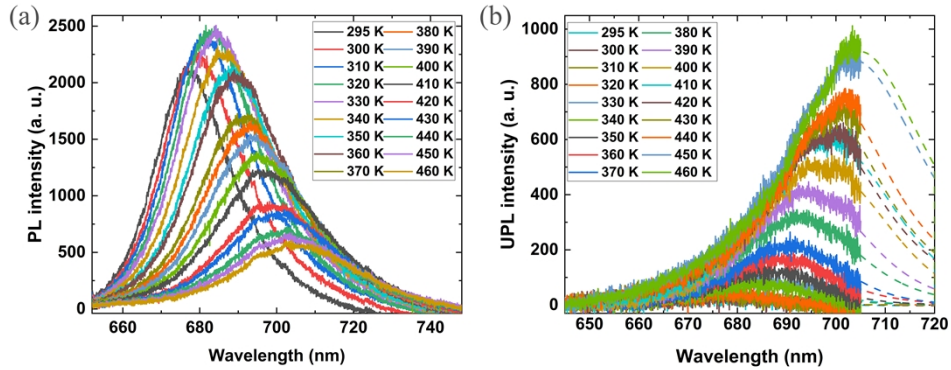
Fig. 3. Temperature-dependent (a) PL spectra excited at 633 nm and (b) UPL spectra excited at 761 nm as temperature increases from 295 K to 460 K.

To further quantitatively analyze the evolution of PL and UPL emission with temperature, the emission peak wavelength and the integrated emission intensity are extracted and plotted in Fig. 4(a) and (b). As presented in Fig. 4(a), both PL and UPL emission peak wavelengths show redshifts as a function of temperature due to the temperature-dependent bandgap variation, which can be described by the modified Varshni equation $E_g(T) = E_g(0) - S \langle \hbar \omega_{AC} \rangle \left[\coth \left(\frac{\langle \hbar \omega_{AC} \rangle}{2 k_B T} \right) - 1 \right]$. $E_g(0)$ is the excitonic transition energy when temperature equals to zero, S is a dimensionless constant representing the electron-phonon coupling strength, $\langle \hbar \omega_{AC} \rangle$ is the average acoustic phonon energy, k_B is the Boltzmann constant [35,36]. For monolayer MoS$_2$, $\langle \hbar \omega_{AC} \rangle$ is 22.5 meV, and S value obtained from the fitting is 2.5 for the PL emission, and 2.7 for the UPL emission. As temperature goes up from 295 K to 460 K, a 27 nm redshift of the emission peak wavelength is obtained for both PL and UPL emission, corresponding to a peak energy shift of 71 meV. As illustrated in Fig. 4(b), the integrated UPL emission intensity grows rapidly with the increasing temperature, and it is enhanced by 62 times at 460 K compared to the intensity at room temperature. The significant enhancement of UPL intensity at elevated temperatures can be understood with the increased phonon population and the reduced phonon numbers involved in the UPL process. The temperature-dependent population of TO phonons can be described by Bose-Einstein statistics $N(T) = [\exp(\hbar \omega_{TO}/k_B T) - 1]^{-1}$. The integrated UPL intensity is expressed as $I_{UPL}(T) \propto N^n(T)$, where $n = \Delta E / \hbar \omega_{To}$ is the number of phonons participating in the multiphonon absorption process, which is determined by the temperature-dependent upconversion energy gain $\Delta E(T)$. At elevated temperatures, the phonon population $N(T)$ in monolayer MoS$_2$ increases, leading to stronger phonon-exciton interactions. Meanwhile, the number of phonons n involved in the UPL process is reduced from approximately 4 to 1 at elevated temperatures. The phonon population analysis agrees well with the measured UPL emission intensity data in Fig. 4(b), which demonstrates the use of temperature control to enhance the phonon-assisted

UPL emission. In contrast to the UPL emission, Fig. 4(d) also displays the measured integrated PL intensity which increases before 330 K due to trion dissociation and transition to exciton, and then decreases afterwards because of exciton dissociation. The process can be described by [37] $I_{PL}(T) = I_0 \left(1 + Be^{-\frac{E_b}{k_B T}}\right) / \left(1 + Ae^{-\frac{E_a}{k_B T}}\right)$, where I_0 is the PL intensity at $T = 0$ K, k_B the Boltzmann constant, A and B are weight factors. E_a is the thermal activation energy that dissociates the free excitons, which is related to the normal thermal quenching process. E_b represents the thermal activation energy for excitons that bound to the defects to be activated or for the trions to self-dissociate and transit to the neutral exciton, which is related to the negative thermal quenching process. The data fitting shows $E_a = 390$ meV and $E_b = 35$ meV for the PL process of monolayer MoS_2. The observed temperature-dependent PL emission corresponds to the competition between negative thermal quenching and normal thermal quenching.
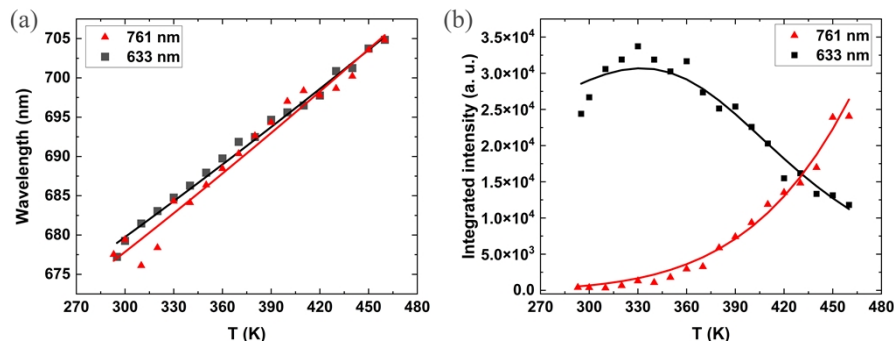
Fig. 4. Evolution of PL and UPL (a) emission peak wavelengths and (b) integrated emission intensity with varying temperature from 295 K to 460 K. Measured PL and UPL data are shown as black squares and red triangles, respectively, while the theoretical fittings are represented by solid lines.

3. Conclusion

In summary, multiphonon-assisted UPL process in monolayer MoS_2 at elevated temperatures has been demonstrated. The observed linear power dependence of UPL intensity indicates the one-photon involved upconversion process at high temperature. At room temperature, upconversion energy gain up to 221 meV is obtained excited by a 761 nm CW laser. As temperature goes up from 295 K to 460 K, the integrated UPL intensity is enhanced by 62 times while the emission peak wavelength is redshifted by 27 nm. Temperature-controlled UPL emission enhancement is analyzed to unveil the contributions of the increased phonon population and the reduced phonon number involved with UPL process at elevated temperatures. The results of high-temperature multiphonon-assisted photon upconversion in atomically thin 2D materials pave the way for many integrated photonics applications such as infrared detection and imaging, nanoscale thermometry, upconversion energy harvesting, and laser cooling.

Disclosures. The authors declare no conflicts of interest.

Data availability. Data underlying the results presented in this paper are not publicly available at this time but may be obtained from the authors upon reasonable request.

References

1. J. Jadczak, L. Bryja, J. Kutrowska-Girzycka, P. Kapuściński, M. Bieniek, Y. S. Huang, and P. Hawrylak, "Room temperature multi-phonon upconversion photoluminescence in monolayer semiconductor WS$_2$," Nat. Commun. **10**(1), 107 (2019).

2. X. Dai, X. Zhang, I. M. Kislyakov, L. Wang, J. Huang, S. Zhang, N. Dong, and J. Wang, "Enhanced two-photon absorption and two-photon luminescence in monolayer MoS$_2$ and WS$_2$ by defect repairing," Opt. Express **27**(10), 13744–13753 (2019).

3. J. Binder, J. Howarth, F. Withers, M. R. Molas, T. Taniguchi, K. Watanabe, C. Faugeras, A. Wysmolek, M. Danovich, V. I. Fal'ko, A. K. Geim, K. S. Novoselov, M. Potemski, and A. Kozikov, "Upconverted electroluminescence via Auger scattering of interlayer excitons in van der Waals heterostructures," Nat. Commun. **10**(1), 2335 (2019).

4. Z. Ye, X. Lin, N. Wang, J. Zhou, M. Zhu, H. Qin, and X. Peng, "Phonon-assisted up-conversion photoluminescence of quantum dots," Nat. Commun. **12**(1), 4283 (2021).

5. Q. Zhang, X. Liu, M. I. Utama, G. Xing, T. C. Sum, and Q. Xiong, "Phonon-Assisted Anti-Stokes Lasing in ZnTe Nanoribbons," Adv. Mater. **28**(2), 276–283 (2016).

6. A. G. del Aguila, T. T. H. Do, J. Xing, W. J. Jee, J. B. Khurgin, and Q. Xiong, "Efficient up-conversion photoluminescence in all-inorganic lead halide perovskite nanocrystals," Nano Res. **13**(7), 1962–1969 (2020).

7. W. Zhang, Y. Ye, C. Liu, J. Wang, J. Ruan, X. Zhao, and J. Han, "Two-Step Anti-Stokes Photoluminescence of CsPbX$_3$ Nanocrystals," Adv. Opt. Mater. **9**(6), 2001885 (2021).

8. T. T. Tran, B. Regan, E. A. Ekimov, Z. Mu, Y. Zhou, W. Gao, P. Narang, A. S. Solntsev, M. Toth, I. Aharonovich, and C. Bradac, "Anti-Stokes excitation of solid-state quantum emitters for nanoscale thermometry," Sci. Adv. **5**(5), eaav9180 (2019).

9. Q. Wang, Q. Zhang, X. Zhao, X. Luo, C. P. Y. Wong, J. Wang, D. Wan, T. Venkatesan, S. J. Pennycook, K. P. Loh, G. Eda, and A. T. S. Wee, "Photoluminescence Upconversion by Defects in Hexagonal Boron Nitride," Nano Lett. **18**(11), 6898–6905 (2018).

10. E. Zuberek, M. Majak, J. Lubczynski, J. Debus, K. Watanabe, T. Taniguchi, C. H. Ho, L. Bryja, and J. Jadczak, "Upconversion photoluminescence excitation reveals exciton-trion and exciton-biexciton coupling in hBN/WS$_2$/hBN van derWaals heterostructures," Sci. Rep. **12**(1), 13699 (2022).

11. X. Shan, F. Wang, D. Wang, S. Wen, C. Chen, X. Di, P. Nie, J. Liao, Y. Liu, L. Ding, P. J. Reece, and D. Jin, "Optical tweezers beyond refractive index mismatch using highly doped upconversion nanoparticles," Nat. Nanotechnol. **16**(5), 531–537 (2021).

12. R. Deng, F. Qin, R. Chen, W. Huang, M. Hong, and X. Liu, "Temporal full-colour tuning through non-steady-state upconversion," Nat. Nanotechnol. **10**(3), 237–242 (2015).

13. M. Pourmadadi, E. Rahmani, M. Rajabzadeh-Khosroshahi, A. Samadi, R. Behzadmehr, A. Rahdar, and L. F. R. Ferreira, "Properties and application of carbon quantum dots (CQDs) in biosensors for disease detection: A comprehensive review," J. Drug Deliv. Sci. Tec. **80**(1), 104156 (2023).

14. H. Zhou, X. Zeng, A. Li, W. Zhou, L. Tang, W. Hu, Q. Fan, X. Meng, H. Deng, L. Duan, Y. Li, Z. Deng, X. Hong, and Y. Xiao, "Upconversion NIR-II fluorophores for mitochondria-targeted cancer imaging and photothermal therapy," Nat. Commun. **11**(1), 6183 (2020).

15. Q. Wang, Q. Zhang, X. Zhao, Y. J. Zheng, J. Wang, X. Luo, J. Dan, R. Zhu, Q. Liang, L. Zhang, P. K. J. Wong, X. He, Y. L. Huang, X. Wang, S. J. Pennycook, G. Eda, and A. T. S. Wee, "High-Energy Gain Upconversion in Monolayer Tungsten Disulfide Photodetectors," Nano Lett. **19**(8), 5595–5603 (2019).

16. K. V. Krishnaiah, P. Venkatalakshmamma, C. Basavapoornima, I. R. Martin, K. Soler-Carracedo, M. A. Hernandez-Rodriguez, V. Venkatramu, and C. K. Jayasankar, "Er^{3+}-doped tellurite glasses for enhancing a solar cell photocurrent through photon upconversion upon 1500 nm excitation," Mater. Chem. Phys. **199**, 67–72 (2017).

17. K. V. Krishnaiah, P. Venkatalakshmamma, K. Upendra Kumar, P. Haritha, V. Lavin, I. R. Martin, N. Ravi, H. Satish Kumar Reddy, V. Venkatramu, N. K. R. Nallabala, and C. Yuvaraj, "Structure, morphology, photonconversion and energy transfer characteristics of Er^{3+}/Yb^{3+}: BaYF$_5$ nanocrystals synthesized by hydrothermal method for photovoltaics," Ceram. Int. **49**(16), 26879–26889 (2023).

18. P. Babu, I. R. Martin, K. V. Krishnaiah, H. J. Seo, V. Venkatramu, C. K. Jayasankar, and V. Lavin, "Photon avalanche upconversion in Ho^{3+}-Yb^{3+} co-doped transparent oxyfluoride glass-ceramics," Chem. Phys. Lett. **600**, 34–37 (2014).

19. S. T. Ha, C. Shen, J. Zhang, and Q. H. Xiong, "Laser cooling of organic-inorganic lead halide perovskites," Nat. Photonics **10**(2), 115–121 (2016).

20. K. V. Krishnaiah, Y. Ledemi, C. Genevois, E. Veron, X. Sauvage, S. Morency, E. S. de Lima Filho, G. Nemova, M. Allix, Y. Messaddeq, and R. Kashyap, "Ytterbium-doped oxyfluoride nano-glass-ceramic fibers for laser cooling," Opt. Mater. Express **7**(6), 1980–1994 (2017).

21. E. S. de Lima Filho, K. V. Krishnaiah, Y. Ledemi, Y.-J. Yu, Y. Messaddeq, G. Nemova, and R. Kashyap, "Ytterbium-doped glass-ceramics for optical refrigeration," Opt. Express **23**(4), 4630–4640 (2015).

22. K. S. Novoselov, A. K. Geim, S. V. Morozov, D. Jiang, Y. Zhang, S. V. Dubonos, I. V. Grigorieva, and A. A. Firsov, "Electric field effect in atomically thin carbon films," Science **306**(5696), 666–669 (2004).

23. A. K. Geim, "Graphene: status and prospects," Science **324**(5934), 1530–1534 (2009).

24. K. S. Novoselov, V. I. Falko, L. Colombo, P. R. Gellert, M. G. Schwab, and K. Kim, "A roadmap for graphene," Nature **490**(7419), 192–200 (2012).

25. L. Yuan, B. Zheng, J. Kunstmann, T. Brumme, A. B. Kuc, C. Ma, S. Deng, D. Blach, A. Pan, and L. Huang, "Twist-angle-dependent interlayer exciton diffusion in WS$_2$-WSe$_2$ heterobilayers," Nat. Mater. **19**(6), 617–623 (2020).

26. D. Akinwande, N. Petrone, and J. Hone, "Two-dimensional flexible nanoelectronics," Nat. Commun. **5**(1), 5678 (2014).

27. F. H. L. Koppens, T. Mueller, P. Avouris, A. C. Ferrari, M. S. Vitiello, and M. Polini, "Photodetectors based on graphene, other two-dimensional materials and hybrid systems," Nat. Nanotechnol. **9**(10), 780–793 (2014).

28. Q. H. Wang, K. Kalantar-Zadeh, A. Kis, J. N. Coleman, and M. S. Strano, "Electronics and optoelectronics of two-dimensional transition metal dichalcogenides," Nat. Nanotechnol. **7**(11), 699–712 (2012).

29. A. M. Jones, H. Yu, J. R. Schaibley, J. Yan, D. G. Mandrus, T. Taniguchi, K. Watanabe, H. Dery, W. Yao, and X. Xu, "Excitonic luminescence upconversion in a two-dimensional semiconductor," Nat. Phys. **12**(4), 323–327 (2016).

30. A. Mushtaq, X. Yang, and J. Gao, "Unveiling room temperature upconversion photoluminescence in monolayer WSe$_2$," Opt. Express **30**(25), 45212–45220 (2022).

31. M. Manca, M. M. Glazov, C. Robert, F. Cadiz, T. Taniguchi, K. Watanabe, E. Courtade, T. Amand, P. Renucci, X. Marie, G. Wang, and B. Urbaszek, "Enabling valley selective exciton scattering in monolayer WSe$_2$ through upconversion," Nat. Commun. **8**(1), 14927 (2017).

32. C. Lee, H. Yan, L. E. Brus, T. F. Heinz, J. Hone, and S. Ryu, "Anomalous lattice vibrations of single- and few-layer MoS$_2$," ACS Nano **4**(5), 2695–2700 (2010).

33. N. Dong, Y. Li, S. Zhang, N. McEvoy, R. Gatensby, G. S. Duesberg, and J. Wang, "Saturation of Two-Photon Absorption in Layered Transition Metal Dichalcogenides: Experiment and Theory," ACS Photonics **5**(4), 1558–1565 (2018).

34. B. Han, C. Robert, E. Courtade, M. Manca, S. Shree, T. Amand, P. Renucci, T. Taniguchi, K. Watanabe, X. Marie, L. E. Golub, M. M. Glazov, and B. Urbaszek, "Exciton States in Monolayer MoSe$_2$ and MoTe$_2$ Probed by Upconversion Spectroscopy," Phys. Rev. X **8**(3), 031073 (2018).

35. K. P. O'Donnell and X. Chen, "Temperature dependence of semiconductor band gaps," Appl. Phys. Lett. **58**(25), 2924–2926 (1991).

36. S. Tongay, J. Zhou, C. Ataca, K. Lo, T. S. Matthews, J. Li, J. C. Grossman, and J. Wu, "Thermally Driven Crossover from Indirect toward Direct Bandgap in 2D Semiconductors: MoSe$_2$ versus MoS$_2$," Nano Lett. **12**(11), 5576–5580 (2012).

37. H. Shibata, "Negative thermal quenching curves in photoluminescence of solids," Jpn. J. Appl. Phys. **37**(Part 1, No. 2R), 550–553 (1998).